RSC Advances

ROYAL SOCIETY OF CHEMISTRY

www.rsc.org/advances

In situ synthesis of silver nanostructures on magnetic Fe_3O_4@organosilicon microparticles for rapid hydrogenation catalysis

Songfang Zhao[1], Yongju Gao[1, 2], Jinhui Li[1], Guoping Zhang*[, 1], Rong Sun*[, 1], Ching-Ping Wong[3, 4]

[1]Shenzhen Institutes of Advanced Technology, Chinese Academy of Sciences, Shenzhen 518055, China

[2]Nano Science and Technology Institute, University of Science and Technology of China (USTC), Suzhou 215123, China

[3]School of Materials Science and Engineering, Georgia Institute of Technology, 771 Ferst Drive, Atlanta, Georgia, 30332, United States

[4]Department of Electronic Engineering, Faculty of Engineering, The Chinese University of Hong Kong, Hong Kong

Abstract

Novel protocol to prepare multifunctional magnetic organic-inorganic nanostructured catalyst of Fe_3O_4@organosilicon/Ag with tailored properties is developed. Such nanostructure design endows the catalyst with superparamagnetism (11.6 emu g^{-1}), excellent oxidation resistance, and catalytic activity. Fe_3O_4 nanoparticles (NPs) are encapsulated with porous organosilicon via improved self-assembly of flexible-bridged organosilicon precursor without templates. Subsequently, dispersed Ag NPs are *in situ* grown on the porous microparticles via silver mirror reaction. The as-prepared multifunctional catalysts are characterized by scanning electron microscopy, X-ray photoelectron spectroscopy, vibration sample magnetometer, X-ray diffraction, thermal gravimetric analysis, and nitrogen adsorption and desorption, respectively. The resultant hybrid microparticles possess micro- and nano-pores, and exhibit a small hysteresis loop and low coercivity.

Meaningfully, they exhibit exceptional catalytic performance for the reduction of 4-nitrophenol in the presence of sodium borohydride and could be reused at least 9 times with excellent stability by means of convenient magnetic separation. The catalyst could be employed to reduce other dyes such as methylene blue, orange G and rhodamine B, and their corresponding reductions follow pseudo-first-order reaction. Therefore, the proposed structure design and scalable route for the synthesis of hierarchical catalyst can pave the way for synthesizing other catalyst systems to address the diverse reaction demands.

Keywords: magnetically responsive, flexible-bridged, silver mirror reaction, catalytic kinetic order

1. Introduction

Recently, noble-metal (such as Au, Pd, Ag or their alloys) nanoparticles (NPs) have attracted intensive attentions for their unexpected high catalytic activity toward various catalytic reductions, due to their extremely high surface area-to-volume ratio [1-6]. Among them, Ag NPs are one of the most fascinating topics in the consideration of its relatively cheap price, as well as excellent chemical and physical properties. However, there are several major challenges that greatly prohibit Ag NPs from a large-scale use. First, Ag NPs tend to aggregation, which decreases the surface area of Ag NPs, resulting in the degradation of catalytic activity. Second, the separation of Ag NPs from the catalytic reaction systems by centrifugation or filtering is tedious and time-consuming, thus hampering the recovery and reusability of catalysts in aqueous solution. Moreover, the synthesis of Ag NPs always involves various hazardous and toxic reagents such as sodium borohydride and hydrazine hydrate [7-11]. Therefore, a novel design and synthesis of “green” Ag NPs with long-term stability and facile separation is highly desirable.

To overcome these mentioned issues, many methods have been developed to

synthesize magnetically retrievable Ag-based catalyst. Fe_3O_4 magnetic nanoparticles (MNPs), which possess high saturation magnetization, low coercivity and good biocompatibility, could be employed as perfect platforms for loading various nanocatalysts [12-14]. Lin [15] developed dumbbell-like Au-Fe_3O_4 nanostructures as recyclable nanocatalysts for reduction of 4-nitrophenol (4-NP) to 4-aminophenol (4-AP) in the presence of $NaBH_4$. Li [16] reported the preparation of recyclable catalysts Ag/Au-decorated Fe_3O_4/SiO_2 nanoparticles through Au seeds attached onto NH_2-SSCNs, followed by the deposition of Ag for catalytic reduction of methylene blue. However, Fe_3O_4 MNPs are prone to be easily aggregated, oxidized or dissolved in acid medium during the treatment procedure, and the traditional silica layer is non-porous and needs to be modified to loading metal NPs [16-19]. Therefore, a suitable approach to design multifunctional composites consisting of Fe_3O_4 MNPs and other functional components is essential to avoid such limitations. Organosilicon is regarded as one of the efficient coating layer for Fe_3O_4 MNPs due to its high chemical and thermal stabilities, adjustable reactive sites, and good bio-compatibilities [20-22]. On the other hand, organosilicon is also regarded as promising candidate for immobilizing Ag NPs and avoiding the aggregation of Ag NPs [23]. The integrated microspheres of magnetic oxides and noble metals could endow the porous organosilicon with excellent catalytic activity and convenient magnetic separation. In return, the porous organosilicon could immobilize the Ag NPs and enhance the stability of Fe_3O_4 core. In general, it remains a challenge to how to conveniently synthesize these desirable multifunctional structures for extended applications.

In the present work, we propose a facile and scalable approach to deposit Ag NPs on Fe_3O_4 encapsulated with organosilicon (Fe_3O_4@Si/Ag), which is applied to catalytic reduction of diverse dyes. Initially, magnetically responsive Fe_3O_4@Si (core@shell) microparticles are fabricated via solvothermal and improved sol-gel method. Then, Ag NPs are *in situ* grown on the surface of Fe_3O_4@Si microparticles via the silver mirror reaction. The as-prepared Fe_3O_4@Si/Ag catalyst could successfully realize a combination of functions

and features from single component. Furthermore, as a magnetically recoverable catalyst, its catalytic performance, reusability along with the corresponding kinetics behaviours are also investigated in the reduction of 4-NP, orange G, methylene blue, and rhodamine B in the presence of $NaBH_4$. More important, the unique Fe_3O_4@Si hierarchical structure makes the microparticles promising candidates for immobilizing metal catalyst.

2. Materials and Methods

2.1 Materials

Hexamethylene diisocyanate (HDI), 3-aminopropyl triethoxylsilane (APTS), and polyvinylpyrrolidone (PVP) are purchased from Aladdin Reagent Co., Ltd and used as received without any further purification. Sodium borohydride ($NaBH_4$), silver nitrate ($AgNO_3$), iron chloride hexahydrate ($FeCl_3 \cdot 6H_2O$), sodium acetate anhydrous (NaAc), ethylene glycol, glucose ($C_6H_{12}O_6$), orange G (OG), rhodamine B (RhB), methylene blue (MB) and 4-NP are purchased from Sinopharm Chemical Reagent Co., Ltd. Chloroform and ethanol are dried before using. Other chemicals are analytical grade and used without any further purification. Milli-Q grade water is used in all experiments.

2.2 Synthesis of Fe_3O_4 MNPs

The ethanol dispersible Fe_3O_4 MNPs are synthesized according to previous method [24]. Briefly, $FeCl_3$ $6H_2O$ (1.5 g, 5.56 mmol), PVP (1.0 g, 1 mmol), and NaAc (2.0 g, 24.4 mmol) are dissolved in ethylene glycol (60 mL) with magnetic stirring. The obtained yellow solution is then transferred into a 100 mL Teflon-lined stainless-steel autoclave, sealed and maintained at 200 °C for 8 h. After the reaction is completed, the black precipitates are filtered, washed with ethanol and deionized water 3 times to remove irons possibly remnant. The as-prepared Fe_3O_4 MNPs is then re-dispersed in ethanol (5 wt%), and stored for the next procedure.

2.3 Synthesis of organosilicon-coated Fe_3O_4 (Fe_3O_4@Si) microparticles

The disilylated hexamethylene-bridged organosilicon precursor (DHBP) is synthesized according to our previous work [25]. The product is confirmed through detecting –NCO absorption band at 2275 cm^{-1} by Fourier transform infrared spectroscopy (FTIR). The as-prepared DHBP is then dissolved in dried $CHCl_3$ (34 wt%) and stored for the following procedure.

The organosilicon coated Fe_3O_4 microparticles are prepared under multi-step acid-alkali condition without templates. All glassware is dried completely prior to use. Typically, 6.5 g DHBP/$CHCl_3$ solution (34 wt%) and 6.44 g Fe_3O_4/ethanol solution (5 wt%) are charged into a round bottomed flask equipped with a mechanical stirrer, and the mixture is stirred vigorously for 5 min. Then 0.65 g diluted HCl (0.1 M) is added into the above solution and stirred for another 3 min to obtain uniform solution. Subsequently, 0.07 g HCl (10 M) is then dropwise added to the mixture under ultrasonication condition for 2 min, and a solution of ethanol (10 mL) and $CHCl_3$ (5 mL) is poured to the mixture. After another 5 min 1.5 mL ammonium hydroxide (25 wt%) is added. The reaction is stirred for another 20 min, and then aged for 0.5 h at room temperature. The products are washed with $CHCl_3$, ethanol and water sequentially, and dried in an oven overnight at 60 ^{o}C. It should be noted that the concentration and amount of HCl and NH_4OH should be well controlled.

2.4 Synthesis of silver NPs supported on Fe_3O_4@Si (Fe_3O_4@Si/Ag)

A versatile approach is used to immobilize Ag NPs on the Fe_3O_4@Si particles via silver mirror reaction [26]. A typical procedure is as follows: Fe_3O_4@Si particles (350 mg), deionized water (110 mL) and glucose (0.270 g) are charged into the Erlenmeyer flask equipped with a mechanical stirrer, and the mixture undergoes 10 min of ultrasonication to obtain a dispersed suspension. Fresh $Ag(NH_3)_2OH$ solution is prepared as follows: ammonium hydroxide (0.55 M) is dropwise added into silver nitrate aqueous solution (20 mL, 8 mM) until the

$AgOH/Ag_2O$ precipitate disappears. Subsequently, the fresh $Ag(NH_3)_2OH$ solution is poured into the above mixture. The resultant mixture is stirred for 2.0 h at room temperature. The slurry-like product is magnetically collected and washed with water and ethanol repeatedly to remove any impurities, and the obtained catalysts (Fe_3O_4@Si/Ag) are dried overnight in a vacuum oven at 60 °C.

2.5 Catalytic reduction of various organic dyes

The reduction of organic dyes including OG, RhB, MB and 4-NP is carried out in a quartz cuvette and monitored using an ultraviolet-visible (UV-vis) spectroscopy at room temperature. In a typical catalytic reduction, 35 mL of fresh $NaBH_4$ (10 mM) aqueous solution is added into a glass beaker containing 5 mL 4-NP (0.4 mM) aqueous solution with vigorous stirring, leading to an immediate colour change from yellow to yellow-green. Subsequently, 35 mg of Fe_3O_4@Si/Ag catalyst is added into the above mixture, and meanwhile 3.5 mL of reaction mixture is transferred to a quartz cuvette immediately before UV-vis measurements. Therefore, the obtained data can be designated as the value for reaction time t=0. Afterwards, the mixture is *in situ* monitored by measuring the adsorption at λ_{max}=400 nm every 1 min to detect the reduction evolution. As the reduction proceeds, the peak at λ_{max}=400 nm corresponding to the *p*-nitrophenolate ion disappears and the solution changes gradually from yellow-green to colourless. OG, RhB and MB are reduced by $NaBH_4$ at the similar condition and *in situ* monitored by measuring their adsorption at λ_{max}= 478, 553, 665 nm using a UV-vis spectrophotometer, respectively. As the reaction proceeds, the peaks at λ_{max}= 478, 553, 665 nm disappear. As control experiment, similar reactions have also been performed without Fe_3O_4@Si/Ag catalyst.

To study the recyclability of the magnetic catalysts, the used Fe_3O_4@Si/Ag catalyst is separated from the solution by magnet after the completion of reduction process. Similar to the above catalytic reduction process, the cuvette

is then placed in a UV–vis spectrophotometer to monitor the time-dependent absorption at λ_{max}=400 nm at room temperature. The recycle tests are repeated at least 9 times.

2.6 Measurements and Characterizations

The morphology and structure are characterized using field-emission scanning electron microscope (SEM, FEI Nova Nano SEM 450). FTIR spectra are recorded with KBr pellets on infrared spectrometer (Vertex70, Bruker Optik GmbH, Germany) with the range of 500-4000 cm^{-1}. UV-vis absorption spectra of the samples are recorded on a UV-vis-NIR spectrometer (Shimadzu UV-3000) with a wavelength range of 200-800 nm. Powder X-ray diffraction (XRD) patterns are recorded on an X-ray diffractometer (Rigaku D/Max 2500) with monochromated Cu Kα radiation (λ=1.54 Å) at a scanning rate of 2° min^{-1}. X-ray photoelectron spectroscopy (XPS) measurements are carried out on a Perkin Elmer PHI 5600 spectrometer operating at 10^{-7} Pa. Thermogravimetric analysis (TGA) is carried out on a thermogravimetric analyser (TA Q600, USA) under 100 mL min^{-1} of nitrogen at a heating rate of 10 °C min^{-1} from room temperature to 800 °C. The Brunauer-Emmett-Teller (BET) surface area is determined by nitrogen adsorption and desorption using a specific surface area analyser (Micromeritics ASAP 2020, USA). By using the Barrett-Joyner-Halenda (BJH) model, the pore volumes and pore size distributions are derived from the desorption branches of isotherms. The magnetic properties are carried out on a vibrating sample magnetometer (VSM, Quantum Design MPMS-XL-7) at 300 K and the hysteresis loops are obtained in a magnetic field that varies from -1 to +1 T.

3. Results and discussion

3.1 Synthesis and characterization of Fe_3O_4@Si/Ag catalyst

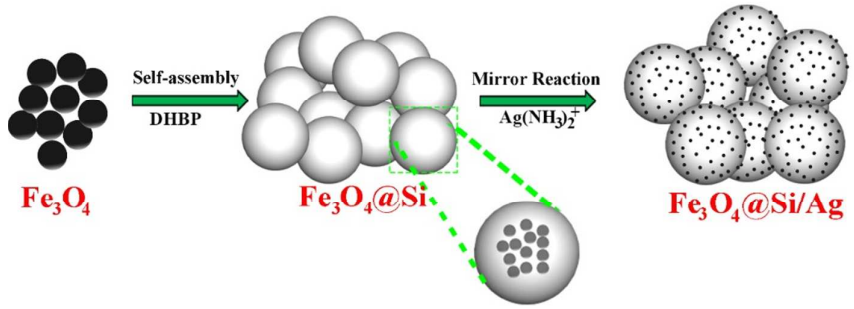

Scheme 1. Schematic illustration for the preparation of Fe_3O_4@Si/Ag catalyst.

As depicted in Scheme 1, the synthesis procedure of magnetic Fe_3O_4@Si/Ag catalyst involves three steps. Firstly, Fe_3O_4 MNPs are synthesized by a solvothermal method via a high temperature reduction of $FeCl_3$ with ethylene glycol as the solvent and reducing agent, NaAc as the precipitation agent, and PVP as the structure-directing agent. Secondly, Fe_3O_4 NPs encapsulated with organosilicon (Fe_3O_4@Si) are obtained due to the fast self-assembly, hydrolysis and condensation of DHBP upon multi-step addition of the diluted HCl and NH_4OH into the mixture. Finally, we employ a simple and green synthesis (silver mirror reaction) for the *in situ* growth of the dispersed Ag NPs on the Fe_3O_4@Si microparticles, due to the high affinity and bonding capacity of amino groups toward silver ions. It should be noted that the design of flexible-bridged precursor and multi-step hydrolysis is helpful to the formation of porous structure.

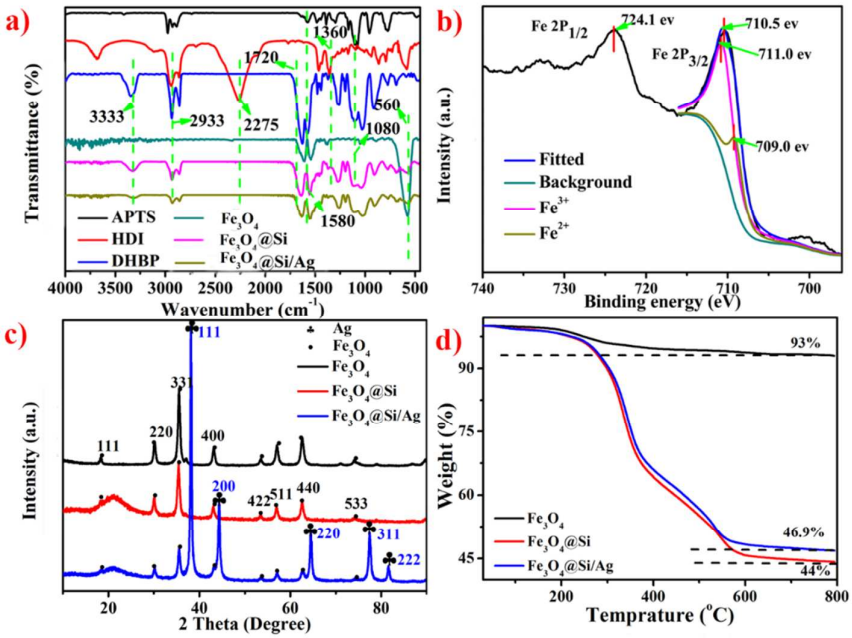

Fig. 1. (a) Evolution of FTIR spectra during the whole synthesis procedure, (b) the X-ray photoelectron spectrum (XPS) of the fitted Fe $2p_{2/3}$ peak from Fe_3O_4 NPs, (c) XRD patterns and (d) TGA curves of Fe_3O_4, Fe_3O_4@Si and Fe_3O_4@Si/Ag.

To characterize the structure variations during the whole synthesis procedure, FTIR spectra are recorded in Fig. 1a. Absorption bands at 2930 and 2850 cm^{-1} are attributed to the asymmetric and symmetric stretching vibration of C-H in aliphatic CH_2 groups, while the peaks at 1580 cm^{-1} result from the bending vibrations of N-H. In the curve of DHBP, the disappearance of peaks at 2275 and 1360 cm^{-1} attributed to stretching vibrations of –NCO, and emergence of a new carboxylic band at 1700–1750 cm^{-1} and a strong peak of the C-O stretching at 1080 cm^{-1} indicate that the reaction between the amine group of APTS and isocyanate group of HDI occurs successfully [27, 28]. The broad absorption peaks at 3333 cm^{-1} corresponding to –OH group indicate the existence of the hydroxyl group. The characteristic peaks at 560 cm^{-1} are assigned the Fe-O stretching vibration of Fe_3O_4, confirming the existence of Fe_3O_4 [29]. Moreover, the spectrum of Fe_3O_4@Si/Ag is almost the same as that of the Fe_3O_4@Si but a weak intensity, resulting from the non-absorption of Ag NPs in the infrared regions [30]. More detailed information regarding the chemical and bonding environment of Fe_3O_4 and Fe_3O_4@Si/Ag is ascertained

using X-ray photoelectron spectroscopy (XPS). The binding energies at 710.5 and 724.1 eV are contributed to the peaks of Fe $2p_{3/2}$ and Fe $2p_{1/2}$ in Fe_3O_4, respectively (Fig. 1b). There are no obvious shakeup satellite structures at the higher binding energy side of both main peaks (about 718.8 and 729.5 eV), which is the characteristic of Fe_3O_4. The relative areas ratio of the deconvoluted peak assigned to Fe^{2+} and Fe^{3+} are calculated to be 0.31:0.69, which is clearly that of the stoichiometric of Fe_3O_4 within the uncertainty of calculations [31]. In the case of Fe_3O_4@Si/Ag, the doublet peaks at 367.8 and 373.8 eV, corresponding to Ag $3d_{5/2}$ and Ag $3d_{3/2}$, and the gap between the two states (6.0 eV), demonstrate that Ag in the composite is zero-valent and further testify that $Ag(NH_3)_2OH$ has been reduced to Ag NPs by silver mirror reaction [32]. Fig. 1c shows the representative XRD patterns of all the samples. The diffraction peaks of Fe_3O_4 NPs can be indexed to the face-centered cubic structures of magnetite. The characteristic peaks at 2θ=18.3°, 30.1°, 35.8°, 43.1°, 53.4°, 57.2°, 62.5° and 74.5°, corresponding to (111), (220), (311), (400), (422), (511), (440) and (533) crystal planes of Fe_3O_4 [8], are observed in all samples, revealing that its crystalline structure is well maintained after a series of functionalization. Besides, the apparent broad peak at around 2θ=23° corresponding to the amorphous peak of organosilicon, indicates that organosilicon has successfully encapsulated the Fe_3O_4 NPs. In the case of Fe_3O_4@Si/Ag catalysts, with the exception of characteristic peaks of Fe_3O_4, five new peaks appearing at 2θ=38.1°, 44.1°, 64.4°, 77.3° and 81.3°, are corresponding to the (111), (200), (220), (311) and (222) crystal planes of the face centered cubic of Ag [10], which prove the formation of Ag NPs and its good crystal structure. These aforementioned results confirm the formation of multifunctional hierarchical catalyst. The thermal behaviors of Fe_3O_4, Fe_3O_4@Si and Fe_3O_4@Si/Ag are assessed by TGA under nitrogen atmosphere in Fig. 1d. It could be seen that the significant weight loss in the range of 200-600 °C is mostly attributed to the degradation of polymer chains of organosilicon and the residual weight increases after the deposition of Ag NPs, which implies that the successful encapsulation of Fe_3O_4 with organosilicon and the immobilization of

Ag NPs.

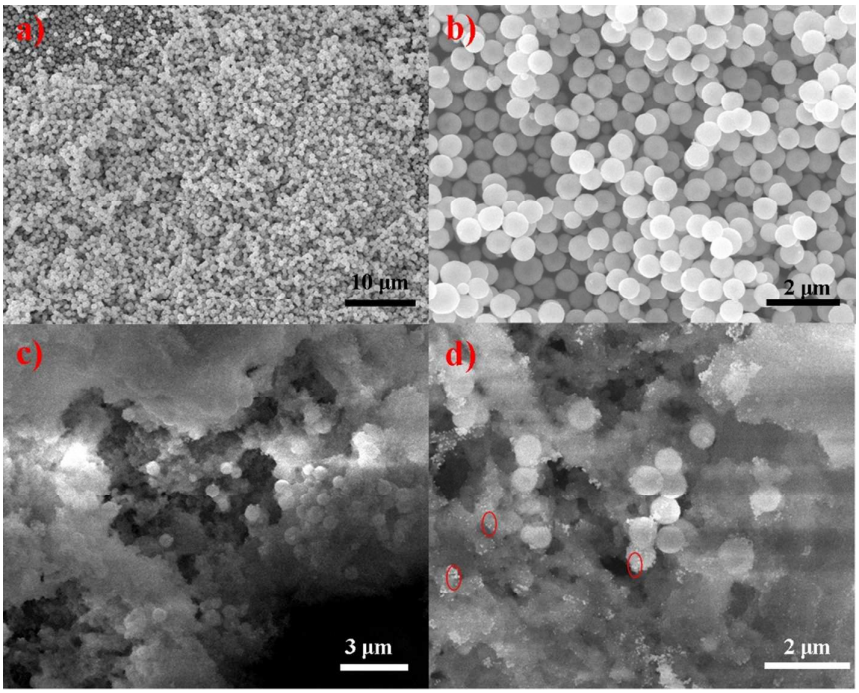

Fig. 2. (a, b) SEM images of Fe_3O_4 NPs, (c) SEM image of Fe_3O_4@Si microparticles, and (d) SEM image of Fe_3O_4@Si/Ag particles, and Ag NPs are marked with ellipses.

The morphologies and structure of Fe_3O_4, Fe_3O_4@Si and Fe_3O_4@Si/Ag are further investigated by SEM (Fig. 2). As revealed in Fig. 2a and b, the Fe_3O_4 microparticles have well-defined spherical morphology with average diameter of 700 nm. Through an improved sol-gel process, the Fe_3O_4 MNPs encapsulated with organosilicon possess rough surface and porous structure, which are not only good platforms for the immobilization of Ag NPs and the multiple accessible channels for diffusion and transport of the reactant molecules, but also improves the oxidation resistance of Fe_3O_4 core. Furthermore, it can be seen that there is no essential structure change after the growth of Ag NPs in the Fe_3O_4@Si/Ag compared with that of Fe_3O_4@Si in Fig. 2d. Therefore, desirable multifunctional structures are successfully developed via a series of processes, including solvothermal method, improved sol-gel method and silver mirror reaction.

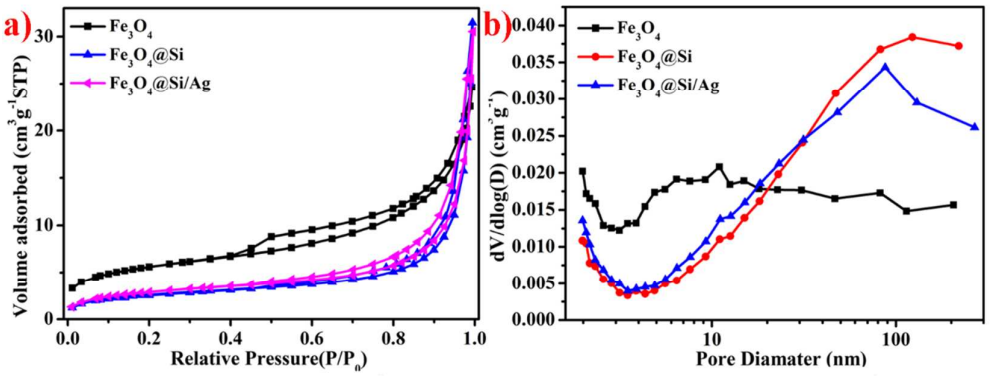

Fig. 3. (a) N_2 adsorption/desorption isotherms and (b) pore size distribution of samples Fe_3O_4, Fe_3O_4@Si and Fe_3O_4@Si/Ag.

To investigate the detailed information of the porous structure in the resultant microparticles, the surface area and pore size distribution are determined by the multipoint BET method using N_2 adsorption/desorption analysis. Fig. 3 shows the N_2 adsorption/desorption isotherms and BJH pore size distribution of Fe_3O_4, Fe_3O_4@Si and Fe_3O_4@Si/Ag. All isotherms can be classified to a type-IV isotherm with H3 hysteresis loop according to the IUPAC and BDDT classification [33]. The BET surface area, pore volume and pore size are summarized in Table S1. These results reveal that there are nano-sized pores, and the primary and secondary pore diameters are centred at 2 and 90 nm (Fig. 3b), respectively, implying that the Fe_3O_4@Si maintains its initial porous structure after the immobilization of the Ag NPs. The decrease in pore size indicates that the Ag NPs occupies the pores of the Fe_3O_4@Si microparticles, and the increase in surface area results from the accumulation of Ag NPs.

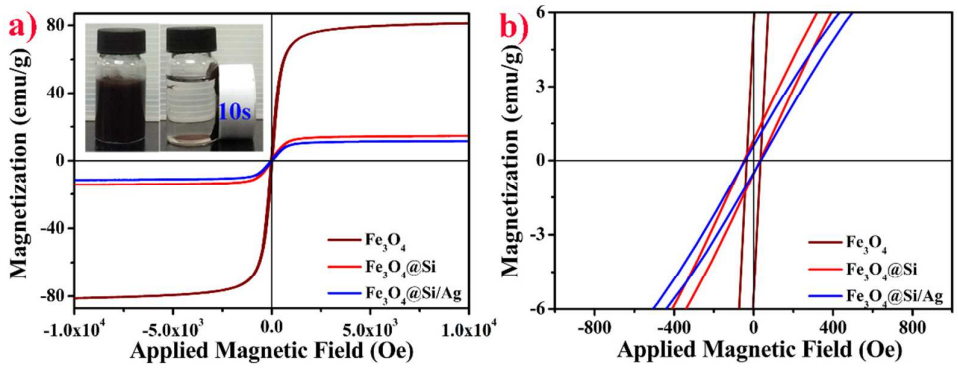

Fig. 4. (a) Room-temperature magnetic hysteresis loops of Fe_3O_4, Fe_3O_4@Si and Fe_3O_4@Si/Ag. The inset shows the response of Fe_3O_4@Si/Ag to an external magnet. (b) Magnification of the magnetic hysteresis loops.

The magnetic behaviours of these materials are critical to ensure magnetic separation. Fig. 4 shows the room-temperature magnetic hysteresis loops of Fe_3O_4, Fe_3O_4@Si and Fe_3O_4@Si/Ag. They exhibit a small hysteresis loop and low coercivity, suggesting superparamagnetic behaviour. The main magnetic parameters of the three samples are listed in Table S2. The magnetic saturation (Ms) values are 81.1, 15.3, and 11.6 emu g^{-1}, respectively, depending on the effective mass of the Fe_3O_4 microspheres. Whereas the coercivity values are 34.9, 43.8, and 47.9 Oe, respectively. The slight changes of coercivity might be attributed to the influence of the surrounding environment [24, 34]. To investigate the magnetic response of the catalyst visually, a magnet is placed beside the cuvette, Fe_3O_4@Si/Ag microparticles in aqueous solution are attracted to the side of the cuvette leaving the solution transparent within 10 s. Therefore, the catalysts could be separated from water quickly under the magnetic field, leading to easy recycling and reuse.

3.2 Catalytic performance

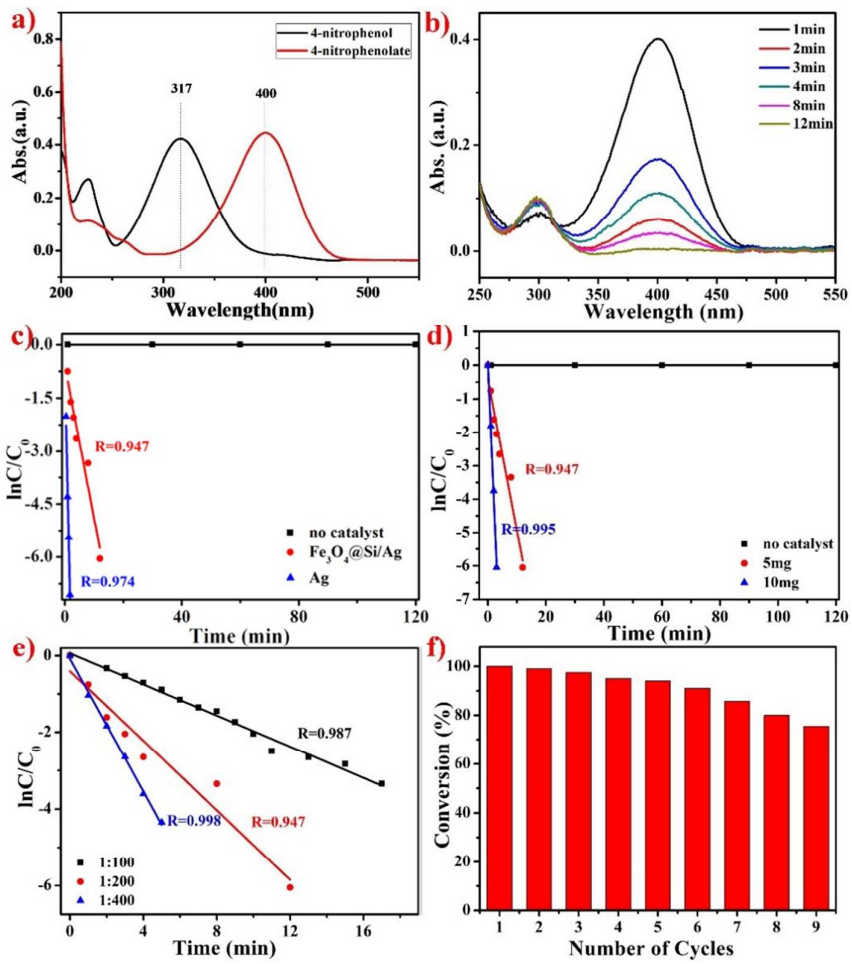

Fig. 5. Catalytic performance of Fe_3O_4@Si/Ag catalyst: (a) UV-vis absorption spectra of 4-NP and 4-nitrophenolate; (b) Time-dependent UV-vis spectra of the reduction of 4-NP to 4-AP by $NaHB_4$ in the presence of Fe_3O_4@Si/Ag; (c) Plots of the ln(C/C_0) vs. reaction time with the addition of Fe_3O_4@Si, Ag NPs and catalyst; (d) Plots of the ln(C/C_0) vs. reaction time with different amount of Fe_3O_4@Si/Ag catalyst; (e) Plots of the ln(C/C_0) vs. reaction time for different mole ratio ($n_{4\text{-NP}}/n_{NaBH4}$); and (f) Recyclability of Fe_3O_4@Si/Ag catalyst for the reduction of 4-NP.

It is well-known that metallic silver nanostructures are excellent catalysts with high activity and selectivity. While immobilized on porous supports, Ag NPs could serve as practical recyclable catalysts towards many reactions. In order to assess the catalytic capability of Fe_3O_4@Si/Ag composites, the reduction of 4-NP, MB, RhB and OG by $NaBH_4$ at room temperature are chosen as model reactions, which are widely used as evaluation criteria of the catalytic activity of metal NPs. The main merit of these reductions is their convenient monitoring by UV-vis absorption spectroscopy because no side reaction exits [35].

As shown in Fig. 5a, upon the addition of $NaBH_4$ aqueous solution, the UV-vis absorbance band immediately shifts from 317 to 400 nm, which is attributed to the formation of 4-nitrophenolate under the alkaline condition. Meanwhile, the corresponding colors change from yellow to yellow green [36]. The reaction conversion can be calculated from C/C_0, which is measured from the relative intensity of UV-vis absorbance (A/A_0) at 400 nm. Herein, C is the concentration of 4-NP during the reaction and C_0 is the initial concentration. It is noteworthy that the reduction of 4-NP with an excess amount of $NaBH_4$ could not occur without suitable catalysts. As shown in Fig. 5b, once introducing a small amount of the Fe_3O_4@Si/Ag catalyst, the peak intensity at 400 nm successfully decreases with concomitant increase in peak at 300 nm as the reduction proceeds, which is the characteristic absorption peak of 4-aminophenol (4-AP), indicating the occurrence of reduction of 4-NP to 4-AP. Meanwhile, the reduction of 4-NP could also be visually witnessed through color change from yellow green to colorless within 12 min. Moreover, the addition of the alone Fe_3O_4@Si cannot promote the reduction of 4-NP even after 120 min and the Ag NPs alone could promote the occurrence of reduction of 4-NP (Fig. 5c), undoubtedly confirming that the reduction of 4-NP by $NaBH_4$ is solely catalyzed by Ag NPs immobilized on Fe_3O_4@Si. That is to say, Ag NPs in the reaction system play an important role in electron transference between the BH_4^- ions and 4-nitrophenolate ions. It is worth noting that the reaction starts immediately without induction time after the addition of catalysts.

The concentration of $NaBH_4$ is higher than that of 4-NP, and it could be considered as constant during the reaction process. Pseudo-first-order kinetics can be applied to evaluate the reaction rate constants. The reaction kinetics can be described as $\ln(C/C_0) = -kt$, where k is the apparent first-order rate constant (min^{-1}) and t is the reaction time (min) [37]. Therefore, we plot $\ln(C/C_0)$ vs. reaction time t in Fig. 5d and e, which show a good linear relationship for $\ln(C/C_0)$ against reaction time t in the catalytic reduction catalyzed by the heterostructures following pseudo-first-order kinetics. The

kinetic reaction rate constant (*k*) calculated from the slope of the straight line in Fig. 5d are 0.0001, 0.453 and 2.010 min^{-1}, respectively. The increase of rate constant directly indicates the speeding up of the degradation of 4-NP, which is attributed to that more catalysts could offer larger surface area and active sites to enhance the contacting opportunity with 4-NP, resulting in the enhancement of catalytic activity. Moreover, the kinetic reaction rate constant (*k*) of the reduction catalyzed by Ag NPs alone is 3.676 min^{-1}, which is higher than that of Fe_3O_4@Si/Ag catalyst due to the effective mass of Ag NPs.

On the other hand, the effect of concentration of $NaHB_4$ aqueous solution on reaction rate constant *k* is also investigated in Fig. 5e. When the mole ratio between the 4-NP and $NaBH_4$ is 100, 200, 400, the corresponding rate constant *k* are calculated to be 0.203, 0.453 and 0.864 min^{-1}, respectively. The increase in rate constant *k* results from the more electrons offered by higher amounts of $NaHB_4$.

In order to demonstrate the universality of Fe_3O_4@Si/Ag catalyst, the catalytic reductions of OG, RhB and MB with $NaBH_4$ have been used as other model reactions. The whole reaction involves the following processes: $NaBH_4$ is adsorbed onto the catalyst surface to form metal hydride, and then various dyes are also adsorbed onto the surface; dyes are reduced and desorbed to create a free space for the reaction to continue. Fig. S2a shows the successive UV-vis spectra of the OG reduction in the presence of Fe_3O_4@Si/Ag. Obviously, the absorption intensity at λ_{max}=478 nm of OG decreases with the reaction time, indicating the occurrence of the reduction of OG. As expected, the catalytic reduction proceeds successfully, and no poisoning of catalyst occurs. Similar to the reduction of 4-NP, reduction of OG also follows pseudo first-order kinetics and exhibits a good linear relationship, as shown in Fig. S2b. The catalyzed reaction rate is determined to be 0.091 min^{-1}, which is ten times higher than that of reduction without catalyst (0.0094 min^{-1}). As for the reduction of RhB and MB, the similar results are obtained, which certifies that the Fe_3O_4@Si/Ag has excellent performance towards the hydrogenation of diversiform dyes under aqueous reaction conditions.

Regeneration capacity of catalyst is of great importance in the view of practical application. Hence, the successive cycles of the catalytic reduction of 4-NP are performed with Fe_3O_4@Si/Ag. After each run of catalysts, the catalysts are separated from the reaction mixture by magnet, rinsed with deionized water, and then reused in the next cycle. As shown in Fig. 5f, in the first three cycles, the conversion is almost 100%; with the increase in cycling times, the conversion drops and still remains at 80% for the same reaction time (5 min), which implies that Fe_3O_4@Si/Ag could serve as a recyclable and reusable catalyst. The recyclability of the catalyst may result from the efficient stabilization of Fe_3O_4@Si/Ag.

4. Conclusion

In summary, the magnetic recyclability of Fe_3O_4, the oxidation resistance and affinity capacity of organosilicon as well as the catalytic activity of Ag NPs are successfully integrated into multifunctional composites through the design of flexible-bridged organosilicon precursor. During the process, the protective layer of porous organosilicon is synthesized via self-assembly, hydrolysis and condensation of DHBP, and the dispersed Ag NPs are *in situ* grown on Fe_3O_4@Si microparticles *via* classical silver mirror reaction. The as-prepared Fe_3O_4@Si/Ag catalysts exhibit enhanced catalytic reactivity and reusability towards the hydrogenation of 4-NP and other dyes. This simple and versatile method can provide a multitude of magnetic catalysts, and the design approach based on Fe_3O_4@Si/Ag may provide a novel platform for the synthesis of other multifunctional organic-inorganic hybrid catalysts for various catalytic applications.

Acknowledgements

This work was financially supported by the National Natural Science Foundation of China (Grant No. 21201175), and Guangdong and Shenzhen Innovative Research Team Program (No.2011D052, KYPT20121228160843692), and R&D Funds for basic Research Program of Shenzhen (Grant No. JCYJ20120615140007998).

References

[1] S. B. Kalidindi and B. R. Jagirdar, *ChemSusChem*, 2012, **5**, 65-75.

[2] F. Zhang, J. Jin, X. Zhong, S. W. Li, J. R. Niu, R. Li and J. T. Ma, *Green Chem.*, 2011, **13**, 1238-1243.

[3] K. Tedsree, T. Li, S. Jones, C. W. Chan, K. M. Yu, P. A. Bagot, E. A. Marquis, G. D. Smith and S. C. Tsang, *Nat. Nanotechnol.*, 2011, **6**, 302-307.

[4] E. Gross, F. D. Toste and G. A. Somorjai, *Catal. Lett.*, 2015, **145**, 126-138.

[5] J. Zhou and Q. Yang, *Chem. Asian J.*, 2012, **7**, 2045-2050.

[6] H. Y. Liu and Q. Yang, *J. Mater. Chem.*, 2011, **21**, 11961-11967.

[7] W. H. Li, X. P. Yue, C. S. Guo, J. P. Lv, S. S. Liu and Y, Zhang, *Appl. Surf. Sci.*, 2015, **335**, 23-28.

[8] B. Duan, F. Liu, M. He and L. N. Zhang, *Green Chem.*, 2014, **16**, 2835-2845.

[9] P. Cronholm, H. L. Karlsson, J. Hedberg, T. A. Lowe, L. Winnberg, K. Elihn, I. O. Wallinder and L. Moller, *Small*, 2013, **9**, 970–982.

[10]J. Chen, Z. Guo, H. B. Wang, M. Gong, X. K. Kong, P. Xia and Q. W. Chen, *Biomaterials*, 2013, **34**, 571–581.

[11]X. M. Huang, X. G. Wang, X. S. Wang, X. X. Wang, M. W. Tan, W. Z. Ding and X. G. Lu, *J. Catal.*, 2013, **301**, 217–226.

[12] M. B. Gawande, P. S. Branco and R. S. Varma. *Chem. Soc. Rev.*, 2013, **42**, 3371-3393.

[13] P. Granitzer, K. Rumpf, Y. Tian, G. Akkaraju, J. Coffer, P. Poelt and M. Reissner, *Appl. Phys. Lett.*, 2013, **102**, 193110-193110-4.

[14] X. D. Liu, Z. G. Zhong, Y. F. Tang and B. Y. Liang, *J. Nanomater.*, 2013, **45**, 209-214.

[15] F. H. Lin and R. A. Doong, *J. Phys. Chem. C*, 2011, **115**, 6591-6598.

[16] L. Li, E. S. G. Choo, X. S. Tang, J. Ding and J. M. Xue, *Acta Mater.*, 2010, **58**, 3825-3831.

[17] X. Bao, Z. Qiang, J. H. Chang, W. Ben and J. Qu, *J. Environ. Sci.*, 2014, **26**, 962–969.

[18] F. F. Fang, J. L. You and H. J. Choi, *Adv. Mater. Res.*, 2008, **47**, 201-204.

[19] W. H. Shi, J. X. Zhu, D. H. Sim, Y. Y. Tay, Z. Y. Lu, X. J. Zhang, Y. Sharma, M. Srinivasan, H. Zhang, H. H. Hng and Q. Y. Yan, *J. Mater. Chem.*, 2011, **21**, 3422-3427.

[20] J. Xie, K. Chen, H. Y. Lee, C. J. Xu, A. R. Hsu, S. Peng, X. Y. Chen and S. H. Sun, *J. Am. Chem. Soc.*, 2008, **130**, 7542-7543.

[21] R. S. Kumar, M. Paulpandi, M. ManivelRaja, D. Mangalaraj, C. Viswanathan, S. Kannan and N. Ponpandian, *RSC Adv.*, 2014, **4**, 13409-13418.

[22] S. R. Kumar, L. Marianna, S. Gianni, A. J. Nathanael, S. I. Hong, T. H. Oh, D. Mangalaraj, C. Viswanathan and N. Ponpandian, *Mater. Res. Express*, 2014, **1**, 015015.

[23] S. S. Park, M. S. Moorthy and C. S. Ha, *NPG Asia Mater.*, 2014, **6**, e96.

[24] Q. Yu, A. P. Fu, H. L. Li, H. Liu, R. Lv, J. Q. Liu, P. Z. Guo and X. S. Zhao, *Colloids Surf., A*, 2014, **457**, 288-296.

[25] Y. J. Gao, S. F. Zhao, G. P. Zhang, L. B. Deng, J. H. Li, R. Sun., L. Y. Li and C. P. Wong, J. Mater. Sci., 2015, 50, 3399-3408.

[26] C. D. Jin, J. P. Li, S. J. Han, Q. F. Yao and Q. F. Sun. *J. Alloys Compd.*, 2015, **635**, 300-306.

[27] T. A. Saleh, *Appl. Surf. Sci.*, 2011, **257**, 7746-7751.

[28] V. K. Gupta, S. Agarwal and T. A. Saleh, *J. Hazard. Mater*., 2011, **185**, 17-23.

[29] Z. Z. Wang, S. R. Zhai, B. Zhai, Z. Y. Xiao, F. Zhang and Q. D. An, *New J. Chem.*, 2014, **38**, 3999-4006.

[30] X. Zhang, W. Jiang, Zhou Y, S. Xuan, C. Peng, L. Zong and X. Gong, *Nanotechnology*, 2011, **22**, 375701.

[31] J. Gao, X. Ran, C. Shi, H. Cheng and Y. Su. *Nanoscale*, 2013, **5**, 7026-7033.

[32] S. F. Zhao, Y. J. Gao, G. P. Zhang, L. B. Deng, J. H. Li, R. Sun and C. P. Wong, *Carbon*, 2015, **86**, 225-234.

[33] B. Naik, S. Hazra, V. S. Prasad and N. N. Ghosh, *Catal. Commun.*, 2011, **12**, 1104-1108.

[34] H. L. Li, J .J. Sang, J. H. Zhao, A. P. Fu, H. Liu, M. Xu, G. S. Pang and X. S. Zhao, *New J. Chem.*, 2012, **36**, 2308-2315.

[35] M. Y. Zhu, C. J. Wang, D. H. Meng and G. W. Diao, *J. Mater. Chem. A*, 2013, **1**, 2118-2125.

[36] S. F. Zhao, Y. J. Gao, J. H. Li, G. P. Zhang, C. Y. Zhi, L. B. Deng. R. Sun and C. P. Wong, *ACS Appl. Mater. Interfaces*, 2015, **7**, 6716-6723.

[37] X. Y. Du, J. He, J. Zhu, L. J. Sun and S. S. An, *Appl. Surf. Sci.*, 2012, **258**, 2717-2723.